JACS
JOURNAL OF THE AMERICAN CHEMICAL SOCIETY
Communication
pubs.acs.org/JACS

Aggregation and Interaction of Cationic Nanoparticles on Bacterial Surfaces

Steven C. Hayden,[†] Gengxiang Zhao,[‡,#] Krishnendu Saha,[§] Ronnie L. Phillips,[†] Xiaoning Li,[§] Oscar R. Miranda,[§] Vincent M. Rotello,[§] Mostafa A. El-Sayed,[†] Ingeborg Schmidt-Krey,[†,‡] and Uwe H. F. Bunz*[,†,∥]

[†]School of Chemistry and Biochemistry, Georgia Institute of Technology, 910 Atlantic Drive, Atlanta, Georgia 30332, United States
[‡]School of Biology, Georgia Institute of Technology, 310 Ferst Drive, Atlanta, Georgia 30332, United States
[§]Department of Chemistry, University of Massachusetts, 710 North Pleasant Street, Amherst, Massachusetts 01003, United States
[∥]Organisch-Chemisches Institut, Ruprecht-Karls Universität Heidelberg, Im Neuenheimer Feld 270, 69120 Heidelberg, Federal Republic of Germany

Supporting Information

ABSTRACT: Cationic monolayer-protected gold nanoparticles (AuNPs) with sizes of 6 or 2 nm interact with the cell membranes of *Escherichia coli* (Gram−) and *Bacillus subtilis* (Gram+), resulting in the formation of strikingly distinct AuNP surface aggregation patterns or lysis depending upon the size of the AuNPs. The aggregation phenomena were investigated by transmission electron microscopy and UV−vis spectroscopy. Upon proteolytic treatment of the bacteria, the distinct aggregation patterns disappeared.

Fundamental insight into the interaction of nanoparticles (NPs) with bacterial cell membranes would provide direction in the design of bactericidal agents and sensor systems.[1] The interaction of NPs with bacterial cell membranes, however, is not well understood. No good models concerning how this interaction takes place or the loci to which the NPs are most attracted (if any) have been proposed. Murphy and co-workers[2] demonstrated that Gram+ *Bacillus cereus* coordinates to CTAB-protected gold nanorods, but the coverage of the bacteria was isotropic. Similar observations were made by other groups that investigated the interaction of gold NPs (AuNPs) with microbes to access bioinspired advanced materials.[3] Jiang and co-workers[4a] demonstrated that diaminopyrimidinethiol-functionalized, cationic, 3 nm AuNPs induce the formation of outer membrane vesicles (i.e., blebbing), leading to membrane disruption and uncontrolled release of bacterial DNA in *Pseudomonas aeruginosa*. The antimicrobial activity of these monolayer-protected AuNPs, which was also investigated by Feldheim and co-workers,[4b] is an attractive applicative boon. Depending upon the specific membrane and NP structure, membrane interactions with nanoparticulate matter can result in blebbing, tubule formation,[4,5] or the creation or enlargement of membrane defects, etc.,[6] in a subtle structural interplay of the NP and membrane structures.

We recently reported that conjugates of cationic, hydrophobic, monolayer-protected AuNPs[7] with semiconducting polyelectrolytes are discriminatory materials for proteins,[8] eukaryotic cells,[9] and bacteria.[1a,10] With a small array of differently functionalized AuNPs, different strains of *Escherichia coli* could be discriminated reliably. The negatively charged bacterial surfaces displaced the polyelectrolyte from the quenching AuNPs (**NP2**), yielding differential fluorescence turn-on. This displacement required complexation of the bacteria surface by **NP2**. For a fundamental understanding of these interactions, we investigated the complexes of *E. coli* (XL1 blue) and *Bacillus subtilis* with **NP1** and **NP2** using transmission electron microscopy (TEM) and UV−vis spectroscopy.

We selected a hexyl-substituted, ammonium-functionalized thiol (Figure 1) as a protective coating for our AuNPs, as it

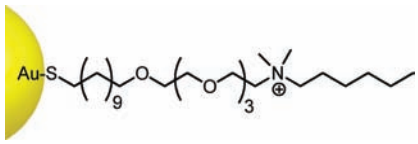

Figure 1. Schematic diagram of monolayer-protected AuNPs used in this study (**NP1**, 6 nm diameter; **NP2**, 2 nm diameter).

interacted optimally with different bacterial species and strains, apparently displaying the correct mix of hydrophobicity and positive charge. We examined AuNPs with diameters of 2 nm (**NP2**) and 6 nm (**NP1**), as the latter display a well-behaved plasmon band upon aggregation. The bathochromic shift of this band correlates with the number and separation distance of interacting NPs. Decreasing the interparticle distance and increasing the number of particles leads to larger shifts, making this a valuable tool for studying aggregation of **NP1** on bacteria in suspension.

NP1 particles were obtained from place exchange of undecanethiol-capped AuNPs formed via the heat-induced size evolution method;[11] **NP2** particles were obtained via place exchange of pentanethiol-capped AuNPs formed via the Schiffrin−Brust method.[12] In the first experiment (Figures 2 and 3) **NP1** was mixed with a bacterial suspension of *B. subtilis* or *E. coli* [for details, see the Supporting Information (SI)].

Received: February 5, 2012
Published: April 10, 2012

   dx.doi.org/10.1021/ja301167y | *J. Am. Chem. Soc.* 2012, 134, 6920−6923

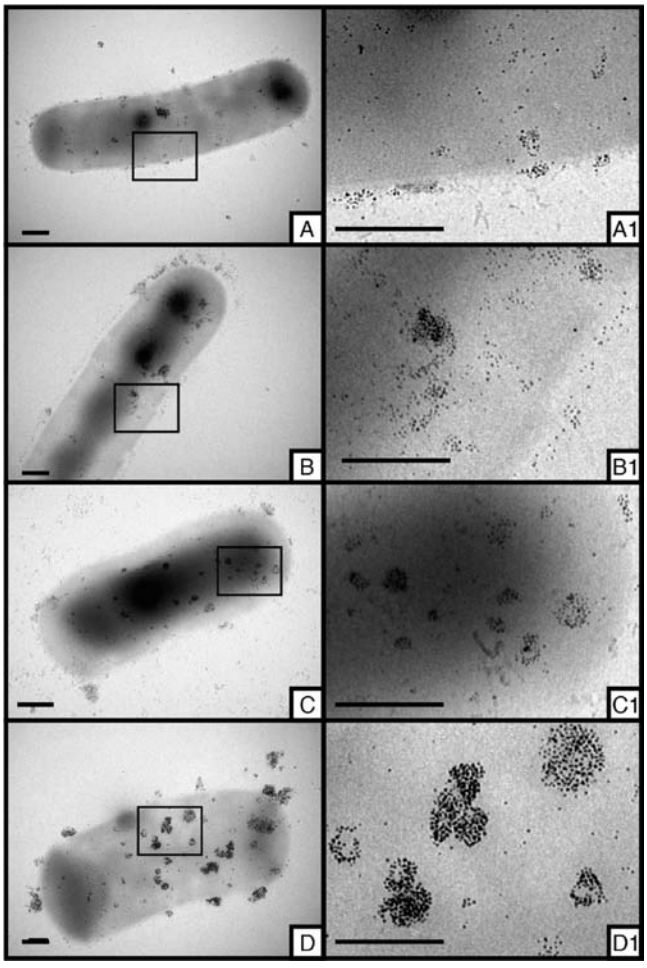

Figure 2. (left) TEM images of timed stages of the interaction of **NP1** with *B. subtilis* with (right) corresponding higher-magnification views of the boxed areas. Images were collected at incubation time points of (A) 20 s, (B) 1.5 min, (C) 3 min, and (D) 10 min. Scale bars are 200 nm. The high-contrast circular regions close to the center of A–C and also in Figure 3A–D) are due to a slight defect in the CCD camera chip and do not overlap with any regions of interest.

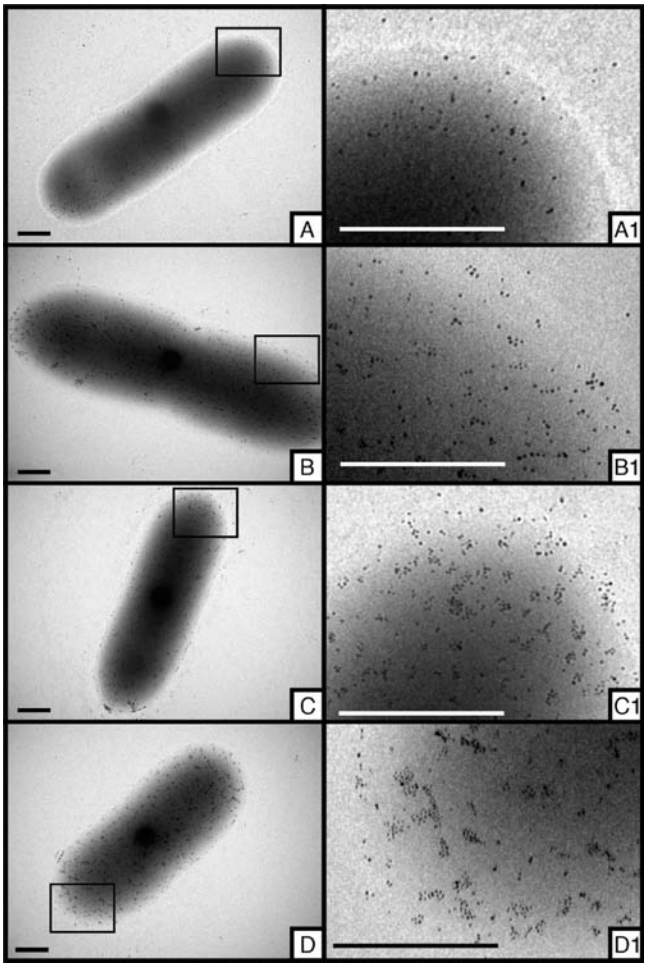

Figure 3. (left) TEM images of timed stages of the interaction of **NP1** with *E. coli* with (right) corresponding higher-magnification views of the boxed areas. Images were collected at incubation time points of (A) 20 s, (B) 1.5 min, (C) 5 min, and (D) 30 min. Scale bars are 200 nm.

Aliquots were removed successively at increasing time intervals, applied to TEM grids, and fixed with 1% uranyl acetate. Imaging (JEOL JEM-1400 transmission electron microscope, Gatan Orius SC1000, Ultrascan 1000 CCD camera) yielded the images shown in the following figures. At the early stages of interaction, only a few **NP1** particles were aggregated on the negatively charged cell membranes of either *B. subtilis* or *E. coli*. Aggregation in *B. subtilis* samples began immediately and progressed more rapidly to full aggregation than in *E. coli* samples. However, all of the bacteria examined showed aggregation patterns. No cell showed a random isolated particle distribution over its surface. **NP1** was found to sit on top of the glycocalix, the tough outer membrane of Gram+ bacteria. With increasing time, the number and size of the discrete aggregates increased, and a striking pattern developed (Figure 2D). The micrographs indicate that **NP1** either clusters on "hot spots" of increased hydrophobicity and/or negative charge density on the bacterial surface or induces hot spots with increased binding to the cell. In Figure 2D, the aggregates have higher contrast, and some of them are located at the periphery on membrane protrusions of the bacterium in this particular image view. Binding apparently occurs at the bacterial surface, and **NP1** particles are not endocytosed or otherwise translocated to the inside of the bacterium.

In *E. coli* samples, the formation of **NP1** aggregates was also seen but was less developed than in *B. subtilis* (Figure 3). Here, at short time intervals, single **NP1** particles appeared to be almost randomly distributed over the body of the bacterium. However, at increased exposure times, aggregation became apparent, though the aggregates were smaller than those observed in *B. subtilis* samples. After 30 min, *E. coli* featured a large number of smaller aggregates that were evenly dispersed over the whole surface of the bacterium. Figures 2 and 3 show typical micrographs in which the interaction of **NP1** with bacterial cells is demonstrated. Control micrographs of **NP1** in fresh and used growth media are presented in the SI.

We next investigated the kinetics of the aggregation phenomena collectively on many bacterial cells. Figure 4A displays the time-dependent UV–vis spectra of a suspension of *B. subtilis* upon mixing with **NP1**. At the beginning, the plasmon band of **NP1** was observed at 532 nm, but after 30 s, the band already displayed a red shift (an indication of plasmonic coupling as nanoparticles approach each other) and an increase in intensity as the large particle aggregates scattered more light. After ca. 5 min, equilibrium was reached; the band now peaked at 559 nm and did not shift further to the red. In

dx.doi.org/10.1021/ja301167y | *J. Am. Chem. Soc.* 2012, 134, 6920–6923

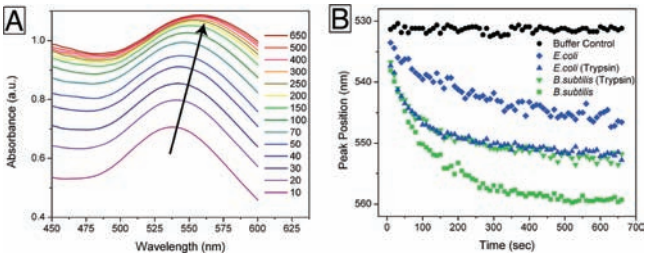

Figure 4. (A) Red shift of the plasmonic peak of **NP1** resulting from aggregation on the cell surface of *B. subtilis* from 10 to 650 s exposure time. The results for *E. coli* are similar but have different final wavelength shift and intensity values (data not shown). (B) Variation of the peak position with time for *E. coli* (blue) and *B. subtilis* (green). Aggregation into clusters proceeds more quickly and results in larger overall cluster formation in *B. subtilis* than in *E. coli*, as evidenced by the shapes of these curves. Symbols: green ▼, trypsin-treated *B. subtilis*; green ■, untreated *B. subtilis*; blue ▲, trypsin-treated *E. coli*; blue ◆, untreated *E. coli*; black ●, buffer.

Figure 4B, the same data are shown, but now the peak wavelength is plotted against time. The analogous experiment was performed for *E. coli* with **NP1**, and the observed shift was considerably less over the same time frame (from 532 to 545 nm), with an ultimate end point of 552 nm after equilibrium was reached at ca. 900 s. This suggests both the formation of significantly smaller aggregates and a decreased rate of aggregate formation. The results from the direct TEM observations and the spectroscopic experiments are therefore mutually reinforcing.

The stark difference in the aggregation behavior of *E. coli* and *B. subtilis* could arise as a result of the different lipid concentrations, the gross constitution of the membranes, or even differences in specific protein complexes that reside on the surface of the bacteria. Also, surface membranes of Gram+ bacteria display a thick peptidoglycan coat and teichoic acids that anchor different proteins, while Gram− bacteria display only a thin peptidoglycan layer, leading to significant physicochemical differences in the two cell-wall types.[13]

To investigate the role of surface proteins in the aggregation phenomena, we examined aggregation on trypsinized *E. coli* and *B. subtilis*. Under these conditions, the cells were still alive but stripped of their surface proteins; the membrane lipid content was unaffected. Figure 5 displays the micrographs of trypsin-

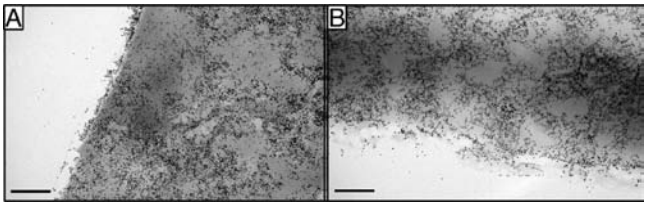

Figure 5. Trypsin-treated (A) *E. coli* and (B) *B. subtilis* after 30 min exposure to **NP1**. Particle binding to the surface is apparent, but the clustering effects seen in untreated cells are markedly absent. Scale bars are 200 nm.

treated *E. coli* and *B. subtilis* after addition of an excess of **NP1**. There was binding of the NPs to the bacterial surfaces, but the clustering disappeared in both cases. Whereas the untreated bacteria exhibited both strain-specific cluster size and strain-specific rate of cluster formation, trypsin-treated cells of the two strains exhibited aggregation kinetics that were almost superimposable (Figure 4b, blue and green triangles), with the same rate of formation and the same final number of coupled particles. This resulted in a rate of surface attachment similar to that seen in *B. subtilis* and a final plasmon shift similar to that observed in *E. coli*. These data suggest that the difference between the surface proteins of *B. subtilis* and *E. coli* is likely responsible for the difference observed in the *clustering* on each strain but has little effect on particle attachment to the surface.

To explore this issue further, we treated both *B. subtilis* and *E. coli* with 2 nm diameter **NP2** particles. Under these conditions, most of the *B. subtilis* cells ruptured, while for *E. coli* (Figure 6), time-dependent aggregation via blebbing occurred.

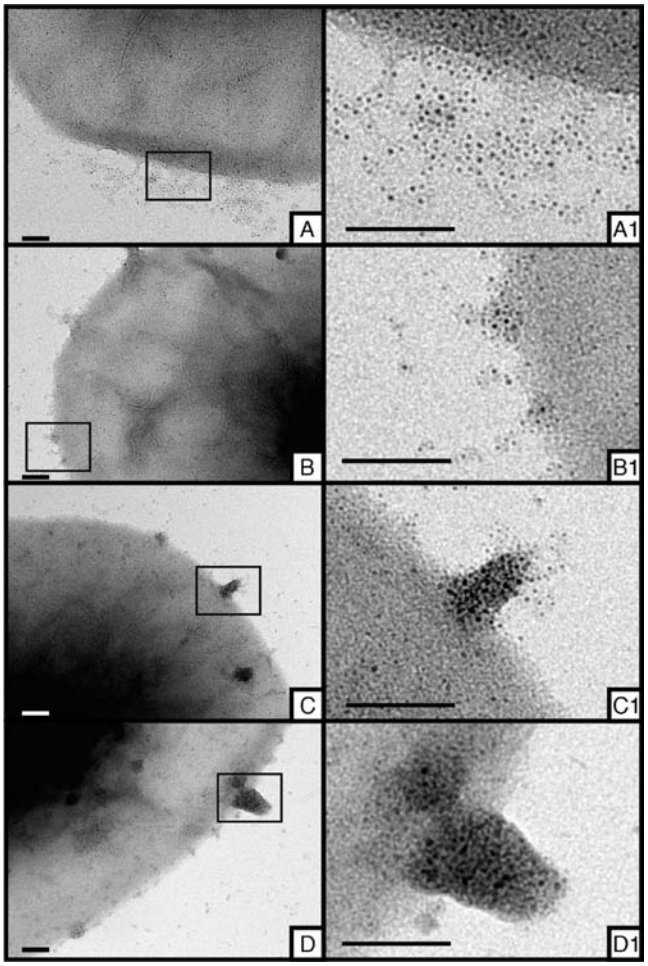

Figure 6. (left) TEM images of the various stages of interaction of **NP2** with *E. coli* showing increased clustering over time, with (right) corresponding higher-magnification views of the boxed areas. Times are (A) 20 s, (B) 1.5 min, (C) 5 min, and (D) 17 min. Scale bars are 50 nm.

Again, at the beginning of the experiment, **NP2** was relatively randomly distributed around the cell membrane of *E. coli* (Figure 6A). After 90 s, formation of protrusions became visible. Additional **NP2** particles congregated around the already-formed blebs. After 5 min, the aggregation process appeared to be finished, and the bacterial cells were spiked with nanoparticle towers that resembled the arrested precursors to the outer membrane vesicles observed in ref 4a.

The rupture of *B. subtilis* in the presence of **NP2** indicates that **NP2** particles are considerably more toxic than the larger **NP1** particles. To investigate this cytotoxicity, both *E. coli* and

dx.doi.org/10.1021/ja301167y | *J. Am. Chem. Soc.* 2012, 134, 6920−6923

B. subtilis were exposed to **NP2** followed by the addition of the substrate mixture (G6P/NADP+/resazurin). Wells containing bacteria and 1× lysis buffer were treated as a positive control (100% membrane damage). The solution mixture was incubated for 5 min at 37 °C, and the resulting fluorescence from the enzymatic reaction was monitored over time using a fluorescent plate reader. We observed a dose-dependent release of Glucose 6-phosphate Dehydrogenase (G6PD, an indicator of membrane damage) from *B. subtilis*, while *E. coli* showed significantly less release over 5 min (SI Figures 7 and 8). We calculated the percentage of lysed cells based on the positive control for both strains and found that after 5 min, ca. 80% of the *B. subtilis* cells had suffered damage from **NP2** (300 nM), while only 20% of the *E. coli* cells were affected. In view of the high degree of curvature witnessed in the interaction of *E. coli* with **NP2**, it is possible that the increased susceptibility of *B. subtilis* to **NP1** may result from *B. subtilis* having only a single cell membrane, whereas *E. coli* has two. This observation underlines the importance of understanding the macroscopic arrangement of molecular species on cell membranes.

In summary, hydrophobic, cationic AuNPs develop spatio-temporal aggregation patterns on Gram+ and Gram− bacteria. The patterns depend upon the nature of the bacterium and the size of the AuNPs. **NP1** particles (6 nm) are nontoxic and aggregate onto specific loci on the bacteria, while **NP2** particles (2 nm) lyse *B. subtilis* but not *E. coli*. The pattern formation might arise because the NPs induce hydrophobic regions on the cell membrane to coalesce or because the NPs aggregate onto hydrophobic, anionic hot spots already present on the bacteria. Regardless, the results are unexpected and defy the notion that cationic NPs must necessarily damage cell walls. There are implications that reach beyond the fundamental modes of interaction between NPs and the cell wall. Cationic AuNPs might work as effective adjuvants to known antibiotics, as they have been shown to modify the cell surface. Additionally, the treatment of multi-drug-resistant infections might benefit from surface-binding NPs.

This study has opened a new window into the aggregation pattern of AuNP on cell walls. Other AuNPs may provide access to a variety of different interaction modes. It also might be possible to detect and explain regions of specific biological activity using binding experiments performed during the infection of a eukaryotic cell by a bacterium or during the cell division of bacterial cells.

■ ASSOCIATED CONTENT

Ⓢ Supporting Information

Complete synthetic procedures, bacteria growth and handling procedures, instrumentation, and cytotoxicity data. This material is available free of charge via the Internet at http://pubs.acs.org.

■ AUTHOR INFORMATION

Corresponding Author

uwe.bunz@oci.uni-heidelberg.de

Present Address

[#]Center for Genetic Medicine Research, Children's National Medical Center, 111 Michigan Ave NW, Washington, DC 20100, United States.

Notes

The authors declare no competing financial interest.

■ ACKNOWLEDGMENTS

We thank the U.S. Department of Energy (Office of Basic Energy Sciences, Division of Materials Sciences and Engineering DE-FG02−04ER46141) for generous funding. We also thank the Doyle lab, in particular M. Rood and B. Azizi, for help with bacteria culturing and M. Johnson for help with TEM grid screening.

■ REFERENCES

(1) (a) Phillips, R. L.; Miranda, O. R.; You, C. C.; Rotello, V. M.; Bunz, U. H. F. *Angew. Chem., Int. Ed.* **2008**, *47*, 2590. (b) Rosi, N. L.; Mirkin, C. A. *Chem. Rev.* **2005**, *105*, 1547. (c) Storhoff, J. J.; Mirkin, C. A. *Chem. Rev.* **1999**, *99*, 1849. (d) Daniel, M. C.; Astruc, D. *Chem. Rev.* **2004**, *104*, 293.

(2) Berry, V.; Gole, A.; Kundu, S.; Murphy, C. J.; Saraf, R. V. *J. Am. Chem. Soc.* **2005**, *127*, 17600.

(3) (a) Ho, Y.; Yuan, J.; Su, F.; Xing, X.; Shi, G. *J. Phys. Chem. B* **2006**, *110*, 17813. (b) Zhang, T.; Wang, W.; Zhang, D.; Zhang, X.; Ma, Y.; Zhou, Y.; Qi, L. *Adv. Funct. Mater.* **2010**, *20*, 1152. (c) Kahraman, M.; Zamaleeva, A. I.; Fakhrullin, R. F.; Culha, M. *Anal. Bioanal. Chem.* **2009**, *395*, 2559.

(4) (a) Zhao, Y.; Cui, Y.; Liu, W.; Ma, W.; Jiang, X. *J. Am. Chem. Soc.* **2010**, *132*, 12349. (b) Bresee, J.; Maier, K. E.; Boncella, A. E.; Melander, C.; Feldheim, D. L. *Small* **2011**, *7*, 2027.

(5) Stachowiak, J. C.; Hayden, C. C.; Sasaki, D. Y. *Proc. Natl. Acad. Sci. U.S.A.* **2010**, *107*, 7781.

(6) (a) Leroueil, P. R.; Hong, S. Y.; Mecke, A.; Baker, J. R.; Orr, B. G.; Banaszak-Holl, M. M. *Acc. Chem. Res.* **2007**, *40*, 335. (b) Leroueil, P. R.; Berry, S. A.; Duthie, K.; Han, G.; Rotello, V. M.; McNerny, D. Q.; Baker, J. R.; Orr, B. G.; Banaszak-Holl, M. M. *Nano Lett.* **2008**, *8*, 420.

(7) (a) Shenhar, R.; Rotello, V. M. *Acc. Chem. Res.* **2003**, *36*, 549. (b) Agasti, S. S.; Rana, S.; Park, M. H.; Kim, C. K.; You, C. C.; Rotello, V. M. *Adv. Drug Delivery Rev.* **2010**, *62*, 316.

(8) You, C. C.; Miranda, O. R.; Gider, B.; Ghosh, P. S.; Kim, I. B.; Erdogan, B.; Krovi, S. A.; Bunz, U. H. F.; Rotello, V. M. *Nat. Nanotechnol.* **2007**, *2*, 318.

(9) Bajaj, A.; Miranda, O. R.; Kim, I. B.; Phillips, R. L.; Jerry, D. J.; Bunz, U. H. F.; Rotello, V. M. *Proc. Natl. Acad. Sci. U.S.A.* **2009**, *106*, 10912.

(10) Bunz, U. H. F.; Rotello, V. M. *Angew. Chem., Int. Ed.* **2010**, *49*, 3268.

(11) (a) Hostetler, M. J.; Templeton, A. C.; Murray, R. W. *Langmuir* **1999**, *15*, 3782. (b) Teranishi, T.; Hasegawa, S.; Shimizu, T.; Miyake, M. *Adv. Mater.* **2001**, *13*, 1699.

(12) Brust, M.; Walker, M.; Bethell, D.; Schiffrin, D. J.; Whyman, R. *J. Chem. Soc., Chem. Commun.* **1994**, 801.

(13) Scott, J. R.; Barnett, T. C. *Annu. Rev. Microbiol.* **2006**, *60*, 397.